Supporting Information for "A new lithospheric density and magnetic susceptibility model of Iran, starting from high resolution seismic tomography"

G. Maurizio[1], C. Braitenberg[1], D. Sampietro[2], M. Capponi[2]

[1]Department of Mathematics and Geosciences, University of Trieste, via Weiss 1, Trieste

[2]Geomatics Research & Development s.r.l., c/o ComoNExT, Via Cavour 2, Lomazzo (CO)

Contents of this file

Introduction

The following Support information includes two textual chapters (S1, S2) and three figures (Fig. S1, Fig. S2, Fig. S3,). In Text S1 we describe the theory behind the Bayesian inversion, reporting the posterior distribution equation. In Text S2 we explain the second inversion performed on the shallowest part of the model to resolve the residual after the first Bayesian inversion, discussed in Sec. 5 of the main text. In Fig. S1 the results of the second inversion are reported, clarified in Text S2. In Fig. S2 we compare the initial average crustal shear modulus with the shear modulus resulting after the inversion. In Fig. S3 we show the depth differences between the base sediment, the Moho and the Curie isotherm surfaces of the model before and after the inversion.

S1. Joint Gravity and Magnetic Bayesian Inversion

The Bayesian inversion approach used to calculate the final 3D model is based on the principles discussed in Sansó and Sampietro (2021) with extensions for simultaneous gravity and magnetic field inversion as delineated in Sampietro et al. (2022). The algorithm is not new and has been intensively tested with simulated and real data (see Sampietro et al. (2021); Sampietro and Capponi (2021a,b); Capponi et al. (2022); Sampietro et al. (2023); Sampietro and Capponi (2023)). We present core ideas here, and direct readers seeking in-depth knowledge to the mentioned references.

The main advantage of the Bayesian inversion technique lies in its ability to estimate the 3D distributions of both density and magnetic susceptibility, and concurrently recover primary geological unit geometries within a specified area, while adhering to a set of imposed constraints. In our solution, the investigated volume is modelled by a set of discrete volumetric elements (voxels). For each voxel, denoted as V_i (where i ranges from 1 to N), we consider three unknowns: its density ρ_i, its magnetic susceptibility χ_i, and a "label" L_i assigning the voxel to a specific geological category (such as water, sediment, crust, etc.) from a predetermined set. Note that while ρ_i and χ_i are continuous, L_i is a discrete variable, where each value represents a category. As a consequence, the vector of all unknown parameters is represented as $\mathbf{x} = \{\rho_i, \chi_i, L_i\}$ for $i = 1 \ldots N$. By leveraging Bayes' theorem in its classical form:

$$P(\mathbf{x}|\mathbf{y}) \propto \mathcal{L}(\mathbf{y}|\mathbf{x})P(\mathbf{x}) \tag{S1.1}$$

we can deduce the posterior distribution $P(\mathbf{x}|\mathbf{y})$ for $\mathbf{x}$, given observed data $\mathbf{y}$. In the above equation, $\mathcal{L}$ represents the likelihood, i.e. the probability of observing $\mathbf{y}$ when $\mathbf{x}$ is given, while $P(\mathbf{x})$ summarises our a-priori probability on $\mathbf{x}$.

This last term is derived by creating an initial model for $\mathbf{x}$ exploiting regional studies, maps, scientific papers, seismic imaging, seismic velocities, well logs, etc. The same source of information can also be used to determine the uncertainty of this preliminary model, allowing us to create a prior probability function for $P(\mathbf{x})$. In the case of the considered joint gravity and magnetic field Bayesian inversion the posterior distribution is given by:

$$
\begin{aligned}
P\left(\rho, \chi, \mathbf{L} \mid \boldsymbol{\Delta g}^{o}, \boldsymbol{\Delta B}^{o}\right) \propto \exp\{&-\left(\boldsymbol{\Delta g}^{o}-\mathrm{A}_{g} \boldsymbol{\rho}\right)^{T} \mathrm{C}_{\Delta g}^{-1}\left(\boldsymbol{\Delta g}^{o}-\mathrm{A}_{g} \boldsymbol{\rho}\right)-\left(\boldsymbol{\Delta B}^{o}-\right. \\
&- \mathrm{A}_{B} \boldsymbol{\chi})^{T} \mathrm{C}_{\Delta B}^{-1}\left(\boldsymbol{\Delta B}^{o}-\mathrm{A}_{B} \boldsymbol{\chi}\right)-\frac{1}{\boldsymbol{\sigma}_{\rho_{\ell}}^{2}}\left(\boldsymbol{\rho}-\overline{\boldsymbol{\rho}}_{\ell}\right)^{T}\left(\boldsymbol{\rho}-\overline{\boldsymbol{\rho}}_{\ell}\right)-\frac{1}{\boldsymbol{\sigma}_{\chi_{\ell}}^{2}}\left(\boldsymbol{\chi}-\overline{\boldsymbol{\chi}}_{\ell}\right)^{T}\left(\boldsymbol{\chi}-\overline{\boldsymbol{\chi}}_{\ell}\right)- \\
&- s^{2}\left(\boldsymbol{L}, \boldsymbol{\ell}^{o}\right)-q^{2}\left(\boldsymbol{L}\right)\} \cdot \delta_{\left[\overline{\rho}_{\ell} \mid 3 \sigma_{\rho_{\ell}}^{2}\right]}(\boldsymbol{\rho})\, \delta_{\left[\overline{\chi}_{\ell} \mid 3 \sigma_{\chi_{\ell}}^{2}\right]}(\boldsymbol{\chi})
\end{aligned}
$$

$$(\text{S1.2})$$

Where $\boldsymbol{\Delta g}^{o}$ and $\boldsymbol{\Delta B}^{o}$ are the vectors of observed gravity and magnetic anomalies respectively, with their associated error covariance matrices $\boldsymbol{C_{\Delta g}}$ and $\boldsymbol{C_{\Delta B}}$. A_{g} and A_{B} are the forward modelling operators, converting densities and magnetic susceptibilities, $\boldsymbol{\rho}$ and $\boldsymbol{\chi}$, into gravity anomalies and total magnetic field intensity, respectively. The expected densities and their variability for the label ℓ are denoted by $\overline{\boldsymbol{\rho}}_{\ell}$ and $\boldsymbol{\sigma}_{\rho_{\ell}}^{2}$, while $\overline{\boldsymbol{\chi}}_{\ell}$ and $\boldsymbol{\sigma}_{\chi_{\ell}}^{2}$ are analogous terms for magnetic susceptibility. s and q are regularising factors that act in geological unit terms.

Eq. S1.2 is complex due to its non-linearity, non-convexity, and the large number of unknowns. This makes the visualisation or the sampling of the a-posteriori probability extremely demanding from the computational point of view. Our chosen strategy is to pinpoint the parameter sets $\boldsymbol{\rho}$, $\boldsymbol{\chi}$, and $\boldsymbol{L}$ that maximise the posterior distribution. This is achieved using a simulated annealing algorithm coupled with a Gibbs sampler, as detailed

in Rossi (2017). For a comprehensive discussion on this optimisation approach, the readers can consult Sections 9.6 and 9.7 of Sansó and Sampietro (2021).

Since the sampling process for $\boldsymbol{\rho}$, $\boldsymbol{\chi}$, and $\boldsymbol{L}$ is probabilistic, the simulating annealing process can be reiterated using different random seeds, analogous to performing indepen- dent inversions. Each iteration yields a potentially distinct 3D model, ideally close to the true maximum of the a-posteriori probability. Our ultimate output is deduced by computing the modal label for each voxel and the mean values for density and magnetic susceptibility. The variance in the values obtained further provides an estimate of the precision of the model output.

S2.   Gravity and Magnetic Inversion of the Shallower Layers

In the main text of Section 5, the gravity and magnetic field fitting after the inversion are shown (Figs. 10c and 10d), i.e. the difference between the observed data and the effect of the final 3D model. As pointed out in the text, the algorithm has been able to fit almost completely the observations with residual of 7 mGal and 15 nT (in terms of standard deviation). However, a set of localised anomalies is clearly visible in both the gravity and magnetic field residuals. This is because the algorithm, given the regional constraints in terms of considered geological units, uncertainties, and smoothness of geometries and densities, was unable to properly fit the gravity data. In other words, these localised residuals could also be seen as an indication that the regional a-priori modelling needs to be locally improved in certain areas in order to fit the observed gravity and magnetic field. This would require a careful analysis of possible local geological formation that is beyond the scope of the current work. We therefore limit ourselves in estimating the order

of magnitude (in terms of density and magnetic susceptibility) of possible sources that explain the residuals. This has been done by exploiting again the Bayesian inversion. In this case, however, we start from our final 3D regional model, fix all the geometries, and allow changes only in the density and the magnetic susceptibility distributions in the first 10 km of the model. We note that in that specific scenario, in which no geometries are involved in the inversion, the Bayesian algorithm is theoretically equivalent to a classical Li-Oldenburg inversion Li and Oldenburg (1996, 1998). The results of this inversion as average density and susceptibility distribution in the first 10 km are reported in Fig. S1

References

Capponi, M., D. Sampietro, J. Ebbing, and F. Ferraccioli. 2022. Antarctica 3-d crustal structure investigation by means of the bayesian gravity inversion: the wilkes land case study. *Geophysical Journal International 229*(3): 2147–2161 .

Li, Y. and D.W. Oldenburg. 1996. 3-d inversion of magnetic data. *Geophysics 61*(2): 394–408 .

Li, Y. and D.W. Oldenburg. 1998. 3-d inversion of gravity data. *Geophysics 63*(1): 109–119 .

Rossi, L. 2017. *Bayesian gravity inversion by Monte Carlo methods.* Ph.D. Thesis, Politecnico di Milano, Milano, Italy.

Sampietro, D. and M. Capponi. 2021a. Gravity for lithosphere architecture determination and analysis: the central eastern mediterranean case study. *Geophysical Prospecting 70*(1): 173–192 .

Sampietro, D. and M. Capponi. 2021b. Seismic constrained gravity inversion: A reliable tool to improve geophysical models away from seismic information. *Geosciences 11*(11):

467 .

Sampietro, D. and M. Capponi. 2023. A novel approach for bathymetry estimation through bayesian gravity inversion. *Geosciences 13*(8): 223 .

Sampietro, D., M. Capponi, and G. Maurizio. 2022. 3d bayesian inversion of potential fields: The quebec oka carbonatite complex case study. *Geosciences 12*(10): 382 .

Sampietro, D., M. Capponi, K. Oikonomopoulos, D. Ktenas, E. Tartaras, and A. Stefatos 2021. 3d model of south crete offshore area by seismic constrained gravity inversion. In *Third EAGE Eastern Mediterranean Workshop*, Volume 2021, pp. 1–3. European Association of Geoscientists & Engineers.

Sampietro, D., M. Capponi, E. Thébault, and L. Gailler. 2023. An enhanced view on the mediterranean sea crust from potential fields data. *Scientific Reports 13*(1): 8298 .

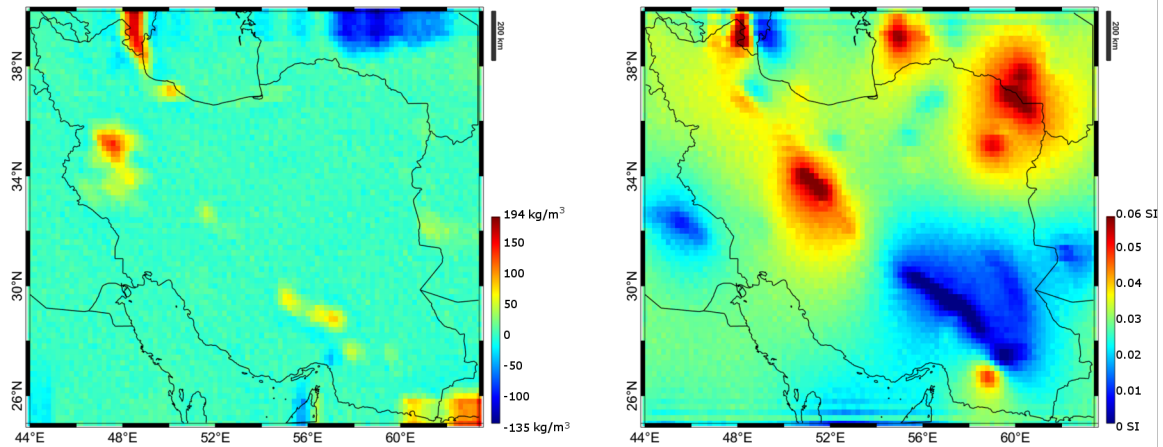Sansó, F. and D. Sampietro. 2021. Analysis of the gravity field: Direct and inverse problems.

Figure S1. Density (left) and magnetic susceptiblity (right) correction in the upper 10 km to the inverted model required to explain the gravity and magnetic residuals after regional Bayesian inversion.
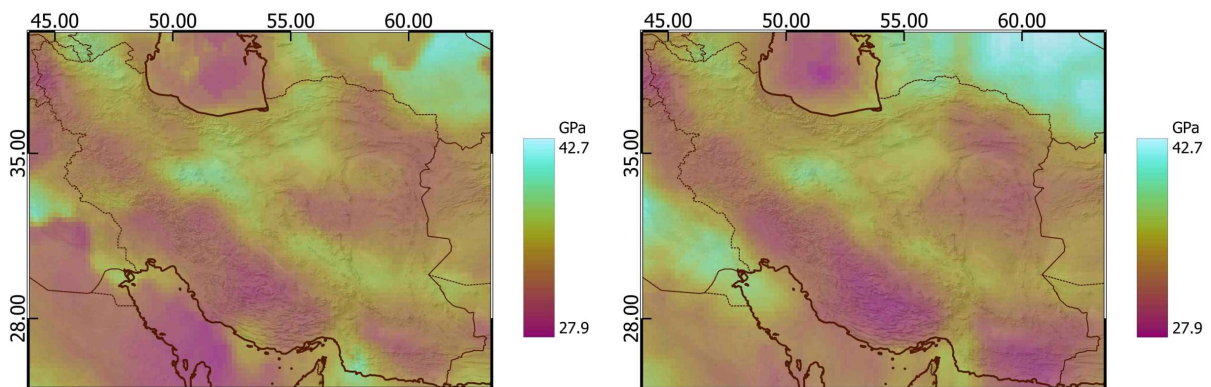

Figure S2. Comparison of the starting average crustal shear modulus (left) to the final crustal shear modulus (right). The final shear modulus is found to be more homogeneous over geologically coherent units.
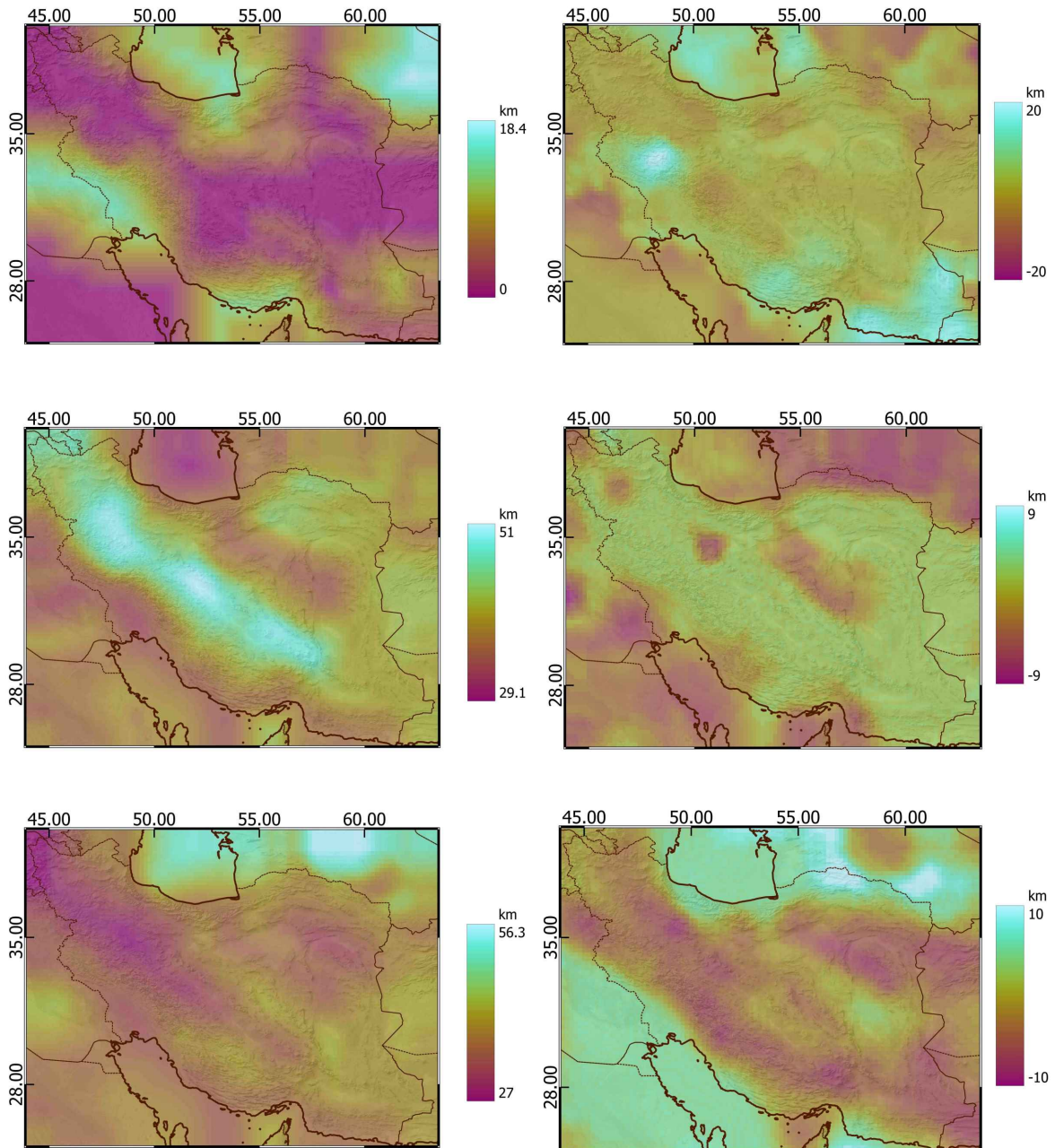
Figure S3. Depths of bottom sediments, Moho, and Curie isotherm surface (top to bottom rows) resulting after the inversion (left) and difference between final and starting models (right). Differences are calculated subtracting the final model from the initial model.